JOURNAL OF SOLID STATE CHEMISTRY **127,** 186–201 (1996)
ARTICLE NO. 0375

Isolation of β-Ag_3AsSe_3, $(Me_3NH)[Ag_3As_2Se_5]$, $K_5Ag_2As_3Se_9$, and $KAg_3As_2S_5$: Novel Solid State Silver Thio- and Selenoarsenates from Solvento-thermal Synthesis

Mercouri G. Kanatzidis and Jun-Hong Chou

Department of Chemistry and Center for Fundamental Materials Research, Michigan State University, East Lansing, Michigan 48824

Received February 26, 1996; in revised form August 22, 1996; accepted August 26, 1996

Three new solid state silver selenoarsenates and one thioarsenate prepared from hydro- and methanothermal synthesis are described. β-Ag_3AsSe_3 (I) and $(Me_3NH)[Ag_3As_2Se_5]$ (II) were synthesized hydrothermally at 110°C from a mixture of $AgBF_4/3K_3AsSe_3$ and $AgBF_4/3K_3AsSe_3/6Me_3NHCl$, while $K_5[Ag_2As_3Se_9]$ (III) and $K[Ag_3As_2S_5]$ (IV) were synthesized methanothermally at 110°C from a mixture of $AgBF_4/3K_3AsS_3$ and $AgBF_4/3K_3AsSe_3$, respectively. β-Ag_3AsSe_3(I) crystallizes in the orthorhombic space group *Pnma* (No. 62) with a = 8.111(1) Å, b = 11.344(2) Å, c = 20.728(3) Å, Z = 8, V = 1907(1) Å^3. This compound is a new allotrope of α-Ag_3AsSe_3 and has a complex three-dimensional structure composed of distorted trigonal planar and tetrahedral Ag^+ ions and $[AsSe_3]^{3-}$ units. $(Me_3NH)[Ag_3As_2Se_5]$ (II) crystallizes in the triclinic space group $P-1$ (No. 2) with a = 10.119(2) Å, b = 18.010(4) Å, c = 14.932(3) Å, α = 110.20 (1)°, β = 103.98(2)°, γ = 99 99(1)°, Z = 2, V = 729.3(8) Å^3. The $[Ag_3As_2Se_5]_n^{n-}$ anion in (II) has a complex two-dimensional layered structure with tetrahedral Ag^+ ions and $[As_2Se_5]^{4-}$ units. $K_5[Ag_2As_3Se_9]$ (III) crystallizes in the orthorhombic space group *Pnma* (No. 62) with a = 12.599(2) Å, b = 12.607(4) Å, c = 14.067(3) Å, Z = 8, V = 2234(1) Å^3. The $[Ag_2As_3Se_9]_n^{5n-}$ anion in (III) has a two-dimensional layered structure with tetrahedral Ag^+ ions and two different kinds of selenoarsenate units, $[AsSe_4]^{3-}$ and $[As_2Se_5]^{4-}$. $K[Ag_3As_2S_5]$ (IV) also crystallizes in the orthorhombic space group *Pnma* (No. 62) with a = 19.210(2) Å, b = 16.867(2) Å, c = 6.3491(7) Å, Z = 8, V = 2057.2(7) Å^3. The $[Ag_3As_2S_5]_n^{n-}$ anion in (IV) possesses a complicated two-dimensional structure with tetrahedral Ag^+ ions and two kinds of thioarsenate ligands, $[AsS_3]^{3-}$ and $[As_3S_7]^{5-}$. The thermal stability and optical absorption properties of these compounds are reported. © 1996 Academic Press

INTRODUCTION

An interesting set of anionic species which can serve as building units to construct complex multinary solids is that of thioarsenates and thioantimonates $[Pn_xQ_y]^{n-}$ (Pn = As, Sb; Q = S, Se). Several compounds based on these anions have been prepared. The majority of them involve ternary systems associated with alkali metals and organic counterions. For example, Schäfer *et al.* prepared a large number of ternary alkali metal antimony sulfides using the hydrothermal technique, including $Cs_2Sb_8S_{13}$ (1) and $A_2Sb_4S_7$ (2) (A = K, Rb, Cs). Sheldrick *et al.* investigated the $M/Pn/Q$ system (M = alkali metal, Pn = As, Sb, Q = S, Se) using superheated water and methanol and showed that a host of ternary phases can be prepared by reacting alkali metal carbonate with a binary Pn_2Q_3 phases (3). Recently, the same methodology has been extended to tetraalkyl ammonium ions which tend to produce more open frameworks (4). Compounds involving the $[Pn_xQ_y]^{n-}$ thioanions in combination with transition or main group metals are more rare. Kolis *et al.* reported several new thioarsenate and antimonate phases from superheated ethylenediamine, including some with metal ions which bind the thioanions $[AsS_3]^{3-}$ and $[SbS_3]^{3-}$ (5). We approach the chemistry of these polyanions from a polychalcogenide viewpoint. We have shown that the hydrothermal method can be a useful synthetic route to new polychalcogenide compounds (6). Polychalcogenide ligands of various lengths can act as building blocks by connecting metal ions together to form compounds with structures ranging from molecular to polymeric one-dimensional, two-dimensional, and even three-dimensional. Since each member of a Q_x^{2-} chain contains at least two lone pairs of electrons, one or all atoms of the polychalcogenide ligand can bind to metal ions (7). Because the As^- ion is isoelectronic to S (or Se), conceptually, the $[As_xS_y]^{n-}$ anions can be related to the well-known polychalcogenide ligands; see Scheme 1. An excellent example for demonstration of this relationship is found in $(Ph_4P)[SAsS_7]$ (8). The eight-member crown shaped ring is isoelectronic with elemental S_8. Because of the charge on the AsS^- ion, the Ph_4P^+ cation is needed for charge balance. The introduction of the trivalent As ions is expected to dramatically increase the chemical connectivity of these chalcogeno-anions and lead to more elaborated structures.

0022-4596/96 $18.00

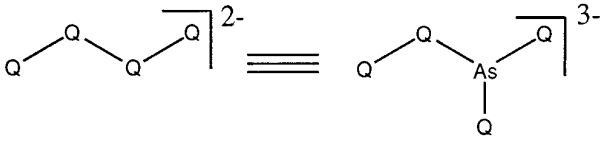

SCHEME 1. The isoelectronic relationship between an Q_4^{2-} and an AsQ_4^{3-} anion.

We have already produced hydrothermally several new metal thioarsenate compounds, including $[InAs_3S_7]^{2-}$ (9), $[BiAs_6S_{12}]^{3-}$ (9), $[HgAs_3S_6]^{-}$ (10), $[Hg_2As_4S_9]^{2-}$ (10), $[Pt(As_3S_5)_2]^{2-}$ (11), and $[Pt_3(AsS_4)_3]^{3-}$ (11). The structures of these compounds range from discrete molecular to one-dimensional chains and two-dimensional layers. In these compounds the $[AsS_3]^{3-}$ anion shows a facile condensation ability resulting in higher nuclearity $[As_xS_y]^{n-}$ units which are found coordinated to the metal cations in an amazing variety of ways. Recently, we have extended this chemistry to selenoarsenate ligands and have reported on $(Me_4N)[HgAsSe_3]$, $(Et_4N)[HgAsSe_3]$, and $(Ph_4P)_2[Hg_2As_4Se_2]$ which are very different from the corresponding sulfides (12a). So far we have prepared only one set of thio- and selenoarsenates with isostructural inorganic anions, $(Me_4N)_2[Mo_2O_2As_2S_7]$ and $(Et_4N)_2[Mo_2O_2As_2Se_7]$ (12b). Interesting results with the corresponding thioantimonates have also been obtained (13).

From our work and that of others it is apparent that, under similar reaction conditions, thioarsenate and selenoarsenate ligands tend to form different $[As_xS_y]^{n-}$ and $[As_xSe_y]^{n-}$ units and, therefore, lead to different structural types. This behavior mirrors the chemical differences observed in pure polychalcogenide chemistry between S_x^{2-} and Se_x^{2-} anions (7). This report details the synthesis, structural and thermal characterization, and optical absorption properties of four new Ag/As_xQ_y (Q = S, Se) polymeric compounds, β-Ag_3AsSe_3 (I), $(Me_3NH)[Ag_3As_2Se_5]$ (II), $K_5[Ag_2As_3Se_9]$ (III), and $K[Ag_3As_2S_5]$ (IV).

EXPERIMENTAL

Chemicals in this work, other than solvents, were used as obtained. All syntheses were carried out under a dry nitrogen atmosphere in a vacuum atmosphere Dri-Lab glovebox except where specifically mentioned.

Optical diffuse reflectance measurements were made at room temperature with a Shimadzu UV-3101PC double beam, double-monochromator spectrophotometer. Thermal Gravimetric Analysis (TGA) was performed on a Shimadzu TGA-50. The samples were heated to 800°C at a rate of 10°C/min under a steady flow of dry N_2 gas. Differential thermal analysis (DTA) was performed with a computer-controlled Shimadzu DTA-50 thermal analyzer. Single crystals (~10.0 mg total mass) were sealed in quartz ampoules under vacuum. An empty quartz ampoule of equal mass was sealed and placed on the reference side of the detector. The samples were heated to the desired temperature at 10°C/min, kept there for 10 min, and then cooled to room temperature at 10°C/min. The reported DTA temperatures are peak temperatures. The DTA samples were examined by powder X-ray diffraction after the experiments. Quantitative microprobe analysis of the compounds was performed with a JEOL JSM-35CF scanning electron microscope (SEM) equipped with a Tracor Northern Energy Dispersive Spectroscopy (EDS) detector. Crystals of each sample were mounted on an aluminum stub which was coated with conducting graphite paint to avoid charge accumulation on the sample surface under bombardment of the electron beam during measurements. The compounds were examined by X-ray powder diffraction to determine phase purity and for identification. Accurate d_{hkl} spacings (Å) were obtained from the powder patterns recorded on a calibrated (with a fresh FeOCl sample as internal standard) Phillips XRG-3000 computer-controlled powder diffractometer with graphite-monochromated Cu$K\alpha$ radiation operating at 35 kV and 35 mA.

Syntheses

K_3AsS_3 (K_3AsSe_3). K_3AsS_3 was synthesized by reacting stoichiometric amounts of alkali metal, arsenic sulfide (selenide), and sulfur (selenium) in liquid ammonia. The reaction gives a yellow (orange) brown powder upon evaporation of ammonia.

β-Ag_3AsSe_3(I). A Pyrex tube (~4 ml capacity) containing $AgBF_4$ (0.02 g, 0.1 mmol), K_3AsSe_3 (0.144 g, 0.3 mmol), Et_4NBr (0.10 g, 0.6 mmol), and 0.3 ml of water was sealed under vacuum and kept at 110°C for 1 day. Large black needle-like crystals with metallic shine were isolated by washing the excess starting material and KCl with H_2O, MeOH, and anhydrous ether. (Yield = 84.5%, based on Ag.) Infrared spectroscopy indicated the absence of organic cations. Semiquantitative microprobe analysis on single crystals gave $Ag_3As_1Se_3$, however the XRD pattern did not match any known Ag/As (or Sb)/Se (or S) ternary phases. The synthetic procedure was later modified to exclude organic cations. The optimized ratio was $1AgBF_4/3K_3AsSe_3$, giving a yield of ~99% based on Ag. Given that another compound with the formula Ag_3AsSe_3 is already known, we will refer to our compound as β-Ag_3AsSe_3 and to the known phase as α-Ag_3AsSe_3 (14).

$(Me_3NH)[Ag_3As_2Se_5]$(II). A Pyrex tube (~4 ml capacity) containing $AgBF_4$ (0.02 g, 0.1 mmol), K_3AsSe_3 (0.144 g, 0.3 mmol), Me_4NCl (0.10 g, 0.6 mmol), and 0.3 ml of water was sealed under vacuum and kept at 110°C for 1 day. A few large dark-red transparent plate-like crystals were isolated by washing with H_2O, MeOH, and anhydrous ether. Although we started with Me_4N^+ as the cation, the

TABLE 1
Crystallographic Data for β-Ag_3AsSe_3, $(Me_3NH)[Ag_3As_2Se_5]$, $K_5[Ag_2As_3Se_9]$, and $K[Ag_3As_2S_5]$

Formula	I Ag_3AsSe_3	II $C_3H_{10}NAg_3As_2Se_5$	III $K_5Ag_2As_3Se_9$	IV $KAg_3As_2S_5$
F. w.	635.41	928.25	1346.65	672.55
a, Å	8.111(1)	10.54991)	12.599(2)	19.210(2)
b, Å	11.344(2)	11.477(2)	12.607(3)	16.867(2)
c, Å	20.728(3)	6.5491(8)	14.067(3)	6.3491(7)
α, deg.	90.00	104.94(1)	90.00	90.00
β, deg.	90.00	107.40(8)	90.00	90.00
γ, deg.	90.00	88.78(1)	90.00	90.00
Z, V, Å^3	12, 1901(1)	2, 729.6(4)	8, 2234(1)	8, 2057.2(7)
Space group	*Pnma*(No. 62)	$P-1$(No. 2)	*Pnma*(No. 62)	*Pnma*(No. 62)
color, habit	black, needle	dark red, plate	black, block	brown, needle
d_{calc}, g/cm^3	6.64	4.22	4.00	4.34
Radiation	Mo$K\alpha$	Mo$K\alpha$	Mo$K\alpha$	Mo$K\alpha$
μ, cm^{-1}	311.11	207.65	215.77	133.00
$2\theta_{max}$, deg.	45.0	45.0	45.0	45.0
Absorption correction	ψ-scan	ψ-scan	ψ-scan	ψ-scan
Transmission factors	0.86–1.04	0.80–1.32	0.51–1.00	0.89–1.18
Index ranges	$0 \le h \le 12$, $0 \le k \le 2$, $0 \le l \le 9$	$0 \le h \le 13$, $-14 \le k \le 14$, $-8 \le l \le 8$	$0 \le h \le 14$, $0 \le k \le 14$, $0 \le l \le 15$	$0 \le h \le 18$, $0 \le k \le 21$, $0 \le l \le 7$
No. of data collected	1791	2027	1856	1723
Unique reflections	1676	1901	1703	1627
Data used ($F_0^2 > 3\sigma(F_0^2)$)	760	997	843	768
No. of variables	106	107	97	106
Final R^a/R_w^b, %	6.7/7.9	4.4/4.7	4.0/4.5	4.0/4.7

[a] $R = \Sigma(|F_o| - |F_c|)/\Sigma|F_o|$.
[b] $R_w = \{\Sigma w(|F_o| - |F_c|)^2/\Sigma w|F_o|^2\}^{1/2}$.

presence of Me_3NH^+ was confirmed by infrared spectroscopy and was further proved by synthesizing the compound in >90% yield with $[Me_3NH]^+$ as the counterion.

$K_5[Ag_2As_3Se_9]$(III). A Pyrex tube containing $AgBF_4$ (0.02 g, 0.1 mmol), K_3AsSe_3 (0.144 g, 0.3 mmol), Ph_4PBr (0.419 g, 1 mmol), and 0.5 ml of methanol was sealed under vacuum and kept at 110°C for 1 week. Large black block-like crystals were isolated by removing the excess starting material and KCl with H_2O, MeOH, and anhydrous ether (yield = 75% based on Ag). Quantitative microprobe analysis on single crystals gave $K_{4.5}Ag_2As_{3.2}Se_{8.6}$. The synthetic procedure was later modified to exclude organic counter-

TABLE 2
Fractional Atomic Coordinates and B_{eq}[a] Values for β-Ag_3AsSe_3 with Estimated Standard Deviations in Parentheses

Atom	X	Y	Z	B_{eq}[a] (A^2)
Ag(1)	0.6435(6)	−0.0180(4)	0.6779(2)	1.5(2)
Ag(2)	0.3314(5)	0.1101(4)	0.7155(2)	1.6(2)
Ag(3)	0.8779(6)	−0.0348(4)	0.5601(2)	1.4(2)
Ag(4)	0.7139(6)	0.0714(4)	0.4424(2)	1.9(2)
Ag(5)	0.7766(9)	−0.2500	0.6312(4)	1.3(3)
Se(1)	0.613(1)	0.2500	0.7120(4)	0.7(4)
Se(2)	0.988(1)	−0.2500	0.5318(4)	1.1(4)
Se(3)	0.1200(7)	0.0889(6)	0.6187(3)	1.0(3)
Se(4)	0.4164(7)	−0.0962(5)	0.7686(3)	0.8(3)
Se(5)	0.454(1)	−0.2500	0.6095(4)	0.9(4)
Se(6)	0.6009(7)	0.0837(5)	0.5629(3)	1.1(3)
As(1)	0.748(1)	0.2500	0.6078(4)	0.6(4)
As(2)	0.220(1)	0.2500	0.5539(5)	0.7(4)
As(3)	0.287(1)	−0.2500	0.7082(6)	1.3(4)

[a] $B(\text{eq}) = \frac{4}{3}[a^2B_{11} + b^2B_{22} + c^2B_{33} + ab(\cos\gamma)B_{12} + ac(\cos\beta)B_{13} + bc(\cos\alpha)B_{23}]$.

TABLE 3
Fractional Atomic Coordinates and B_{eq}[a] Values for $(Me_3NH)[Ag_3As_2Se_5]$ with Estimated Standard Deviations in Parentheses

Atom	*X*	*Y*	*Z*	B_{eq}[a] (A^2)
Ag(1)	0.8318(3)	0.1222(2)	0.2789(4)	3.1(1)
Ag(2)	0.6153(2)	−0.0699(2)	−0.025(4)	2.8(1)
Ag(3)	0.9225(3)	0.1580(2)	0.8225(4)	3.8(1)
Se(1)	0.7384(3)	0.2691(2)	0.5915(4)	1.7(1)
Se(2)	1.0396(3)	0.2355(3)	0.2506(4)	1.8(1)
Se(3)	0.5991(3)	0.1693(3)	−0.0333(4)	1.8(1)
Se(4)	0.6182(3)	−0.2114(2)	−0.4170(4)	1.5(1)
Se(5)	0.8387(3)	−0.1161(3)	0.2712(4)	1.8(1)
As(1)	0.5867(3)	0.1183(3)	0.5867(4)	1.5(1)
As(2)	1.1818(3)	0.0856(2)	0.3646(4)	1.5(1)
N	1.235(2)	0.424(2)	0.805(4)	2.8(5)
C(1)	1.271(3)	0.501(3)	0.687(5)	4.0(7)
C(2)	1.332(4)	0.422(4)	1.005(6)	6.2(9)
C(3)	1.105(5)	0.452(4)	0.855(7)	6.7(9)

[a] $B(\text{eq}) = \frac{4}{3}[a^2B_{11} + b^2B_{22} + c^2B_{33} + ab(\cos\gamma)B_{12} + ac(\cos\beta)B_{13} + bc(\cos\alpha)B_{23}]$.

ions. The optimized reaction ratio of $AgBF_4/K_3AsSe_3$ is 1:3 with the yield close to 90% based on Ag.

$K[Ag_3As_2S_5]$(IV). A Pyrex tube (~4 ml) containing $AgBF_4$ (0.02 g, 0.1 mmol), K_3AsS_3 (0.144 g, 0.3 mmol), Ph_4PBr (0.419 g, 1 mmol), and 0.5 ml of methanol was sealed under vacuum and kept at 110°C for 1 week. Large brown-yellow chunky crystals were isolated by washing the excess starting material and KCl with H_2O, MeOH, and anhydrous ether (yield = 65% based on Ag). Quantitative microprobe analysis on single crystals gave $K_1Ag_{2.5}As_2S_{4.7}$. The procedure was later modified to exclude organic counterions. The optimized reaction ratio of $AgBF_4/K_3AsS_3$ is 1:3 with the yield close to 85% based on Ag.

X-Ray Structure Determination

All compounds were examined with X-ray powder diffraction to check for phase purity and identification. The calculated and observed XRD patterns matched well suggesting (barring any amorphous phases) essentially phase homogeneity.

The single-crystal X-ray diffraction data of all four compounds were collected with a Rigaku AFC6 diffractometer equipped with a graphite-crystal monochromator at 23°C. The data were collected with the $\theta/2\theta$ scan technique. All crystals were stable to the X-ray beam as judged by the intensities of three check reflections measured periodically during the data collection. The space groups were deter-

TABLE 4
Fractional Atomic Coordinates and B_{eq}[a] Values for $K_5[Ag_2As_3Se_9]$ with Estimated Standard Deviations in Parentheses

Atom	*X*	*Y*	*Z*	B_{eq}[a] (A^2)
Ag	0.2369(1)	0.0892(2)	0.7118(2)	2.16(9)
Se(1)	0.3547(3)	−0.2500	0.5712(3)	1.5(2)
Se(2)	0.2825(2)	0.2500	0.8258(3)	1.2(1)
Se(3)	0.0358(2)	0.0958(2)	0.6494(2)	1.4(1)
Se(4)	0.2853(2)	−0.1001(2)	0.7974(2)	1.6(1)
Se(5)	0.0741(3)	−0.2500	0.6552(3)	2.1(2)
Se(6)	0.3781(2)	0.1025(2)	0.5681(2)	1.6(1)
As(1)	0.2481(2)	−0.2500	0.7051(3)	1.1(1)
As(2)	−0.0365(2)	0.2500	0.7165(2)	0.9(1)
As(3)	0.4835(2)	0.2500	0.6010(3)	1.3(2)
K(1)	0.1787(4)	−0.0718(4)	0.4961(4)	2.3(3)
K(2)	0.9796(4)	0.0801(4)	0.1694(4)	2.2(2)
K(3)	0.1707(6)	0.2500	0.4897(7)	2.2(4)

[a] $B(\text{eq}) = \frac{4}{3}[a^2B_{11} + b^2B_{22} + c^2B_{33} + ab(\cos\gamma)B_{12} + ac(\cos\beta)B_{13} + bc(\cos\alpha)B_{23}]$.

TABLE 5
Fractional Atomic Coordinates and B_{eq}[a] Values for $K[Ag_3As_2S_5]$ with Estimated Standard Deviations in Parentheses

Atom	*X*	*Y*	*Z*	B_{eq}[a] (A^2)
Ag(1)	0.6851(1)	0.3690(1)	0.0892(4)	3.1(1)
Ag(2)	0.7332(1)	0.5239(1)	−0.0909(4)	4.2(1)
Ag(3)	0.8572(1)	0.3669(1)	−0.1605(3)	3.3(1)
As(1)	0.7870(2)	0.2500	0.4088(6)	1.0(1)
As(2)	0.5884(1)	0.4603(1)	0.5950(4)	1.2(1)
As(3)	0.6069(2)	0.2500	0.5118(6)	1.0(1)
K	0.4786(3)	0.3776(3)	0.0894(9)	1.8(2)
S(1)	0.3806(4)	0.2500	−0.119(1)	1.4(4)
S(2)	0.8151(3)	0.3558(4)	0.209(1)	1.4(3)
S(3)	0.6071(3)	0.4913(3)	0.256(1)	1.2(2)
S(4)	0.5232(3)	0.3456(3)	0.579(1)	1.1(2)
S(5)	0.6914(3)	0.4075(3)	−0.311(1)	1.2(3)
S(6)	0.6068(5)	0.2500	0.161(1)	1.6(4)

[a] $B(\text{eq}) = \frac{4}{3}[a^2B_{11} + b^2B_{22} + c^2B_{33} + ab(\cos\gamma)B_{12} + ac(\cos\beta)B_{13} + bc(\cos\alpha)B_{23}]$.

mined from systematic absences and intensity statistics. The structures were solved by direct methods of SHELXS-86 (15a) and refined by full-matrix least-squares techniques of TEXSAN (15b) software package of crystallographic program. An empirical absorption correction based on ψ-scans was applied to each data set, followed by a DIFABS (16) correction to the isotropically refined structures. All nonhydrogen atoms except carbon and nitrogen were eventually refined anisotropically. All calculations were performed on a VAXstation 3100/76 computer. Complete data collection parameters and details of the structure solution and refinement are given in Table 1. The fractional atomic coordinates, average temperature factors, and their estimated standard deviations are given in Tables 2 to 5.

Tables of anisotropic thermal parameters and calculated and observed X-ray single-crystal structure factors are available as supplementary material.[1]

RESULTS AND DISCUSSION

Syntheses

At first compound β-Ag_3AsSe_3 (I) was synthesized with tetraethylammonium cations present in the reaction mixture. Although the synthesis can be accomplished without the organic cations in the reaction, only microcrystalline powder was obtained. Single crystals could only be obtained upon addition of tetraethylammonium bromide. The role of the cation is still unclear, but it appears to act as a mineralizer. Given the mild conditions under which it was synthesized, this compound may have eluded mineralogists because it is metastable with respect to the α-form. Traditional sulfosalt synthetic conditions typically involve heating stoichiometric amounts of the elements at temperatures in excess of 1000°C (17) or under more severe hydrothermal conditions than those employed here. The formation of β-Ag_3AsSe_3, from $AgBF_4/3K_3AsSe_3$, in water at 110°C in 1 day suggests that it is only a kinetically stable phase. What is puzzling is that β-Ag_3AsSe_3 is more dense and thus could represent a high pressure modification of α-Ag_3AsSe_3. It would be very interesting to examine the high pressure behavior of the α-form for possible phase transitions.

The compound $(Me_3NH)[Ag_3As_2Se_5]$ (II) was first synthesized by heating $AgBF_4$ with K_3AsSe_3 and Me_4NCl in H_2O at 110°C for 1 day. Because we started with Me_4N^+ as the counterion, we were surprised to observe Me_3NH^+ cations in the structure. Their presence was confirmed with infrared spectroscopy. This cation is not the decomposition product of Me_4N^+ but it appears to exist as ~1% impurity in it. Other closely related organic cations (e.g., $Et_2Me_2N^+$, $EtMe_3N^+$, etc.) were also tried in anticipation of obtaining the same anionic framework, without success, an indication that the Me_3NH^+ ion was playing a critical templating role for this compound. Of course, excellent yields were obtained from Me_3NHCl.

The compound $K_5[Ag_2As_3Se_9]$ (III) was prepared by heating a mixture of $AgBF_4$ and K_3AsSe_3 in methanol at 110°C for several days. Similar reactions with the other alkali metal salts of A_3AsSe_3 (A = Na, Rb) did not yield isostructural $A_5[Ag_2As_3Se_9]$ compounds indicating an important role for K^+.

[1] See NAPS document No. 05347 for 33 pages of supplementary material. This is _____ is not _____ a multi-article document. Order from NAPS c/o Microfiche Publications, P.O. Box 3513, Grand Central Station, N.Y., N.Y. 10163-3513. Remit in advance in U.S. funds only $7.75 for photocopies or $5.00 for microfiche. There is a $15.00 invoicing charge on all orders filled before payment. Outside U.S. & Canada add postage of $4.50 for the first 20 pages and $1.00 for each ten pages of material thereafter, or $1.75 for the first microfiche and 50¢ for each fiche thereafter.

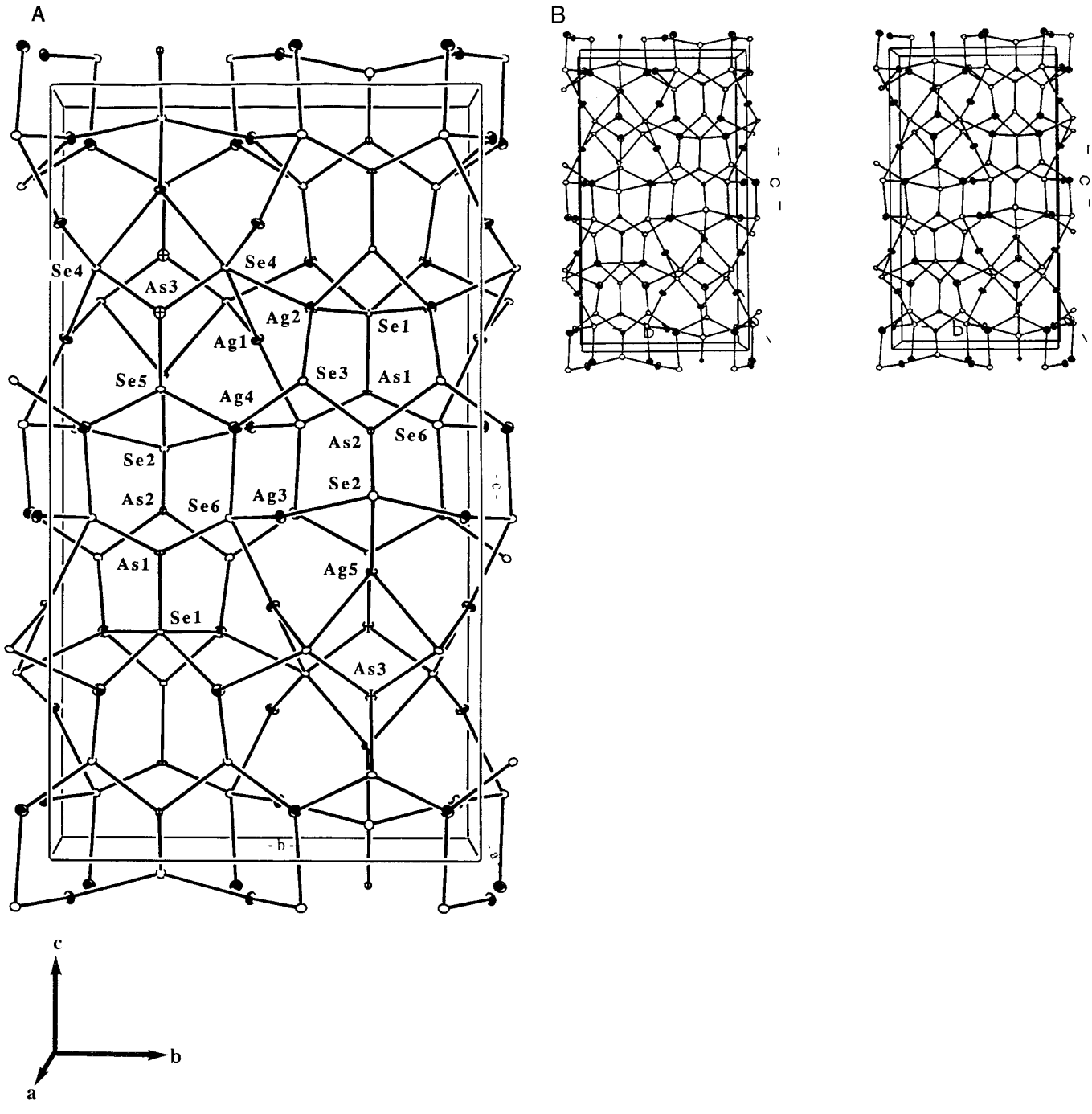

FIG. 1. (A) Structure and labeling scheme of β-Ag_3AsSe_3. (B) Stereoview. Shaded circles are Ag, crossed circles are As, and open circles are Se.

Initial experiments in the Ag/As_xS_y system with water as solvent always yielded the mineral proustite (α-Ag_3AsS_3). By simply changing the solvent from water to methanol this sulfosalt is avoided and the new quaternary phase of $K[Ag_3As_2S_5]$ (IV) is obtained. That this phase is chemically different from (III) suggests, once again, that isostructural Se and S analogs of these compounds would be exceptions, not the rule, in this chemistry.

Structure of β-Ag_3AsSe_3

This compound differs drastically from the α-Ag_3AsSe_3 polymorph (14) and has a remarkably complicated three-

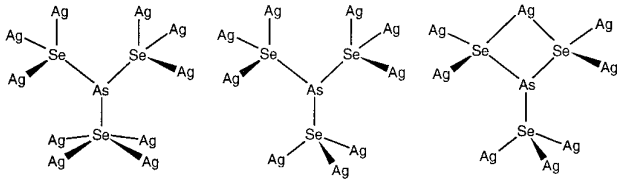

SCHEME 2. The three polydentate binding modes of the $[AsSe_3]^{3-}$ ligand in β-Ag_3AsSe_3.

dimensional, densly packed structure; see Fig. 1A. The connectivity of atoms in this compound can be better appreciated by inspecting the stereoview shown in Fig. 1B. The basic building block of the compound is the $[AsSe_3]^{3-}$ unit which engages in several complex bonding modes in linking the Ag^+ ions together; see Scheme 2. There are also several different environments regarding the Ag^+ ions. The geometry around Ag(1), Ag(3), and Ag(4) is distorted trigonal planar with average Ag–Se bond distances at 2.67(2) Å. The tetrahedral geometry around the Ag(2) is highly distorted with two long Ag(2)–Se(1) bonds, at 2.785(7) and 2.812(8) Å, and two shorter Ag–Se bonds, at 2.651(6) and 2.676(7) Å, respectively. The Se–Ag(2)–Se angles range from 92.8(3)° to 124.3(3)°. The tetrahedral environment around the Ag(5) is even more distorted than that of Ag(2) with two very long Ag–Se ''bonds'' at 2.939(7) Å, and two normal Ag–Se bonds at 2.663(7) and 2.681(9) Å. The Se–Ag(5)–Se angles range from 72.8(3)° to 120.0(3)°. Selected bond distances and angles are given in Tables 6 and 7. There are no bonding Ag–Ag distances in the compound.

Major structural differences between this compound and the rhombohedral structure of α-Ag_3AsSe_3 are the coordination of the Ag^+ ions and their local symmetry. First, the geometry around the Ag atoms in the α-form can best be described as bent-T shaped with the Se–Ag–Se angles ranging from 159° to 85°, while in the β-form the Ag^+ ions are both trigonal planar and tetrahedral, albeit highly distorted. The presence of four coordinate silver atoms is consistent with the fact that the density of β-Ag_3AsSe_3 is 0.12 g/cm^3 higher than that of α-Ag_3AsSe_3. Second, while the pyramidal $[AsSe_3]^{3-}$ units in the structure of the β-form are arranged in a centrosymmetric fashion, those in the α-form stack in columns along the c-axis with their dipoles aligned in the same direction resulting in the acentric space group, $R\,3c$ (No. 161). Therefore, it is hard to deduce a simple structural relationship between the two compounds. However, a polymorphism similar to that observed here has been observed in Cu_3SbS_3. The γ-Cu_3SbS_3 polymorph and the Cu_3SbSe_3 have isomorphous orthorhombic cells which are one-quarter that of β-Ag_3AsSe_3, however, these structures feature only tetrahedral Cu atoms (18).

TABLE 6
Selected Distances (Å) in β-Ag_3AsSe_3 with Standard Deviations in Parentheses

Ag1–Ag2	3.021(6)	Ag3–Se3	2.702(7)
Ag1–Ag3	3.101(6)	Ag3–Se6	2.619(6)
Ag1–Ag2	3.053(5)	Ag4–Se3	2.593(7)
Ag1–Ag5	3.005(6)	Ag4–Se5	2.670(7)
Ag3–Ag4	3.028(6)	Ag4–Se6	2.663(7)
Ag3–Ag5	2.969(5)	Ag5–Se2	2.681(9)
Ag1–Se4	2.778(5)	Ag5–Se4	2.939(7)
Ag1–Se4	2.630(5)	Ag5–Se5	2.659(9)
Ag1–Se6	2.671(7)	As1–Se1	2.421(9)
Ag2–Se1	2.812(8)	As1–Se6	2.418(8)
Ag2–Se1	2.785(7)	As2–Se2	2.451(9)
Ag2–Se3	2.651(6)	As2–Se3	2.408(9)
Ag2–Se4	2.676(7)	As3–Se4	2.389(7)
Ag3–Se2	2.664(5)	As3–Se5	2.450(9)

TABLE 7
Selected Angles (°) in β-Ag_3AsSe_3 with Standard Deviations in Parentheses

Se4–Ag1–Se4	99.5(2)	Ag2–Se3–As2	97.8(3)
Se4–Ag1–Se6	129.1(2)	Ag3–Se3–Ag4	78.1(2)
Se4–Ag1–Se6	131.0(2)	Ag3–Se3–As2	112.8(3)
Se1–Ag2–Se1	102.1(2)	Ag4–Se3–As2	94.9(3)
Se1–Ag2–Se3	124.3(3)	Ag1–Se4–Ag1	137.4(3)
Se1–Ag2–Se3	92.8(3)	Ag1–Se4–Ag2	67.2(2)
Se1–Ag2–Se4	107.3(2)	Ag1–Se4–Ag2	70.2(2)
Se1–Ag2–Se4	115.8(3)	Ag1–Se4–Ag5	157.4(3)
Se3–Ag2–Se4	113.5(3)	Ag1–Se4–Ag5	65.0(2)
Se2–Ag3–Se3	109.4(3)	Ag2–Se4–Ag5	135.3(3)
Se2–Ag3–Se6	139.6(3)	Ag1–Se4–As3	99.7(2)
Se3–Ag3–Se6	110.3(2)	Ag1–Se4–As3	95.7(3)
Se3–Ag4–Se5	127.0(3)	Ag2–Se4–As3	108.1(2)
Se3–Ag4–Se6	132.3(3)	Ag2–Se4–As3	76.6(2)
Se5–Ag4–Se6	99.3(3)	Ag4–Se5–Ag4	98.8(3)
Se2–Ag5–Se4	107.3(3)	Ag4–Se5–Ag5	124.9(2)
Se4–Ag5–Se4	72.8(3)	Ag4–Se5–As3	93.1(3)
Se4–Ag5–Se5	120.0(3)	Ag5–Se5–As3	113.7(4)
Se2–Ag5–Se5	119.9(4)	Ag1–Se6–Ag3	71.8(2)
Ag2–Se1–Ag2	69.5(3)	Ag1–Se6–Ag4	140.3(3)
Ag2–Se1–Ag2	145.5(3)	Ag3–Se6–Ag4	69.9(2)
Ag2–Se1–Ag2	100.4(2)	Ag1–Se6–As1	95.9(3)
Ag2–Se1–Ag2	68.7(3)	Ag3–Se6–As1	89.2(3)
Ag2–Se1–As1	113.2(3)	Ag4–Se6–As1	103.4(3)
Ag2–Se1–As1	101.2(3)	Se1–As1–Se6	97.0(3)
Ag3–Se2–Ag3	132.8(4)	Se6–As1–Se6	102.6(4)
Ag3–Se2–Ag5	67.5(2)	Se2–As2–Se3	100.0(3)
Ag3–Se2–As2	86.0(3)	Se3–As2–Se3	98.7(4)
Ag5–Se2–As2	96.8(4)	Se4–As3–Se4	93.8(3)
Ag2–Se3–Ag3	149.9(3)	Se4–As3–Se5	101.3(3)
Ag2–Se3–Ag4	95.6(2)		

Structure of $(Me_3NH)[Ag_3As_2Se_5]$

The $[Ag_3As_2Se_5]_n^{n-}$ sheets possess a very complicated structure consisting of tetrahedral Ag^+ and $[As_2Se_5]^{4-}$

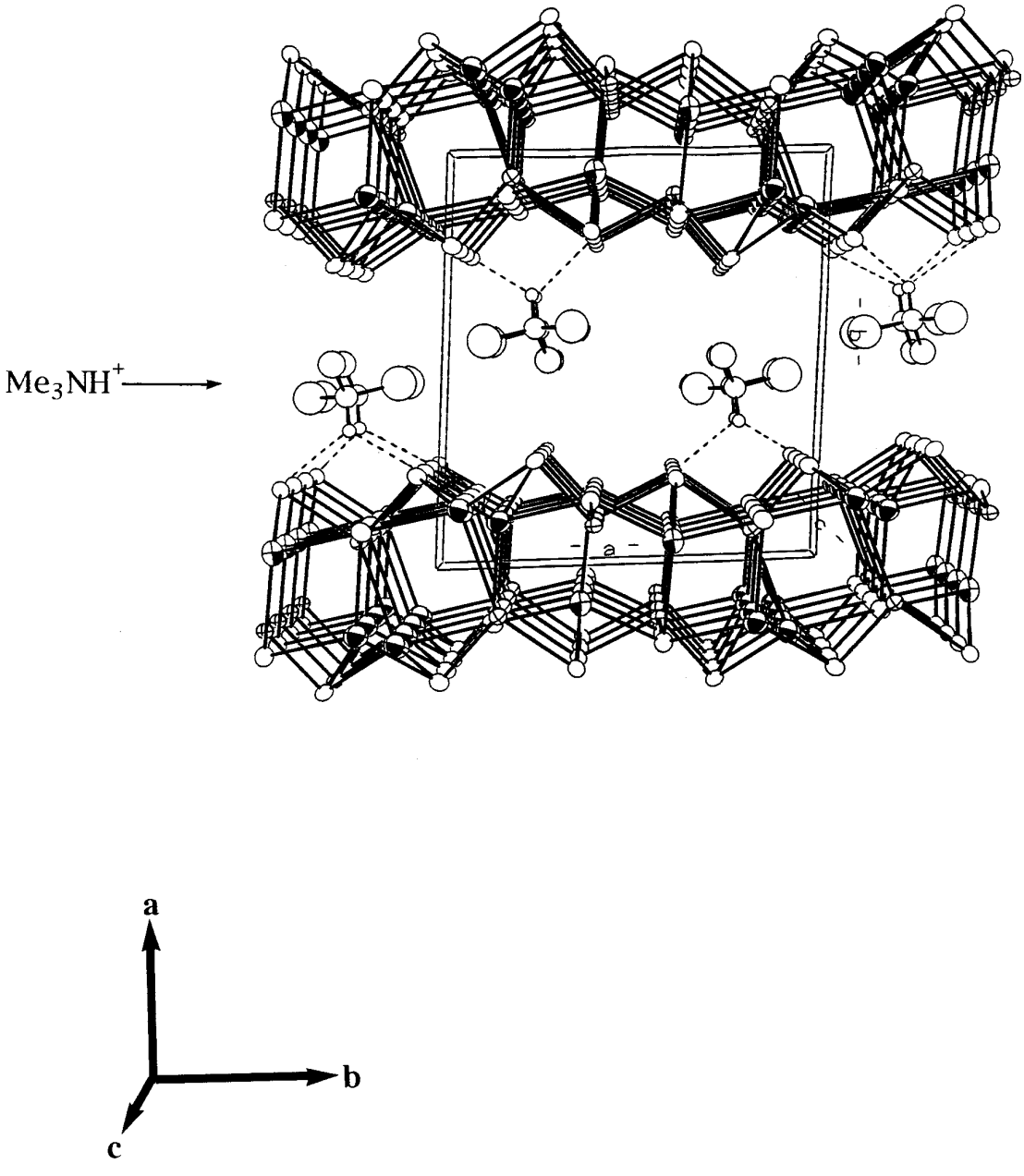

FIG. 2. Packing diagram of $(Me_3NH)[Ag_3As_2Se_5]$. Dotted lines indicate close H---Se contacts <3.5Å.

units; see Figs. 2 and 3. The latter are formed by two-corner-sharing of trigonal pyramidal $[AsSe_3]^{3-}$. The $[As_2Se_5]^{4-}$ unit, which to the best of our knowledge is a new species in a solid state compound, engages in a remarkably complex multidentate coordination involving 11 Ag^+ centers and employing all 5 of its selenium atoms and 1 arsenic atom, see Scheme 3.

The coordination geometry of the Ag(1) and Ag(2) atoms is severely distorted tetrahedral with the Se–Ag–Se bonds angles ranging from 85.9(1)° to 119.8(1)°. The average Ag–Se distance, at 2.725(4) Å, is normal for tetrahedral Ag^+ ions. The Ag(3) atom is coordinated to three Se atoms and the lone electron pair of an As atom. The Ag(3)–As(2) distance is 2.844(4) Å. Only one of the two As atoms in $[As_2Se_5]^{4-}$ is interacting with an Ag center. The direct binding of As in an $[As_xQ_y]^{n-}$ anion to a metal is rare. A similar bonding arrangement was also observed in KCu_2AsS_3 where Cu(1) and Cu(2) were tetrahedrally coordinated to three S atoms and the lone pair of an As atom (19). The average As–Se distance, at 2.410(4) Å, and Se–As–Se

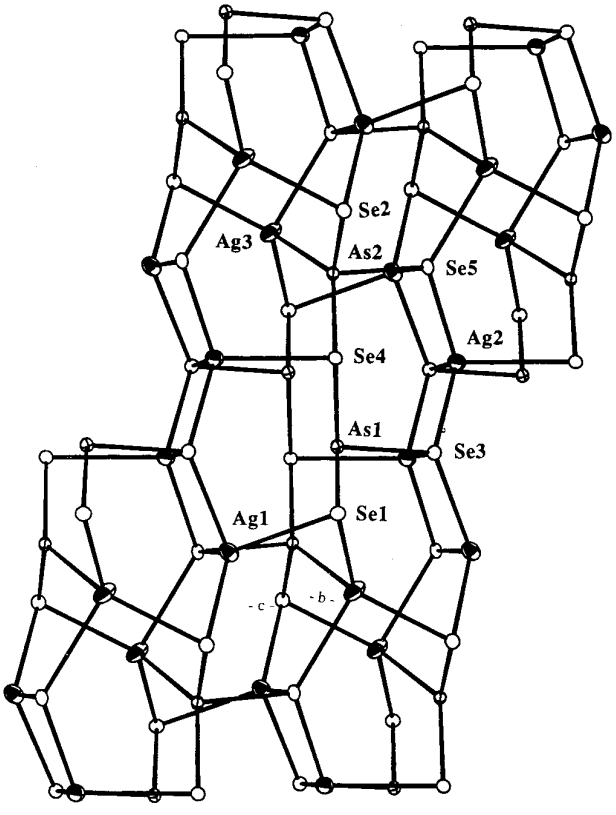

FIG. 3. Structure and labeling scheme of one $[Ag_3As_2Se_5]_n^{n-}$ layer.

angles, at 99.0(1)°, are normal compared to those in other As/Se compounds (20). The shortest Ag–Ag distances are 2.889(5) and 3.012(3) Å and are considered nonbonding. Selected distances and angles are summarized in Tables 8 and 9.

The $[Ag_3As_2Se_5]_n^{n-}$ layers are formed in such way that

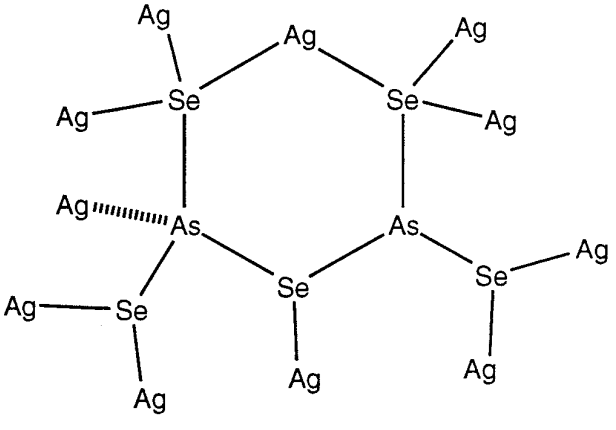

SCHEME 3. Bonding engagement of the polyselenoarsenate unit in (II) with the Ag atoms. The Ag–As interaction is indicated by the dotted line.

TABLE 8
Selected Distances (Å) in the $[Ag_3As_2Se_5]_n^{n-}$ Layer with Standard Deviations in Parentheses

Ag1–Ag2	3.012(3)	Ag3–Se1	2.611(4)
Ag1–Se1	2.713(4)	Ag3–Se2	2.620(4)
Ag1–Se2	2.650(4)	Ag3–Se5	2.770(4)
Ag1–Se3	2.830(4)	Ag3–As2	2.844(4)
Ag1–Se5	2.722(4)	As1–Se1	2.370(4)
Ag2–Ag2	2.889(5)	As1–Se3	2.369(4)
Ag2–Se3	2.802(4)	As1–Se4	2.475(4)
Ag2–Se3	2.653(4)	As2–Se2	2.376(4)
Ag2–Se4	2.790(4)	As2–Se4	2.469(4)
Ag2–Se5	2.638(4)	As2–Se5	2.395(4)

all the lone pairs of the selenium atoms are pointed away from the layers and toward the interlayer space. The Me_3NH^+ ions are located in the gallery region yielding an interlayer distance of 11.47 Å. Interestingly, the hydrogen atom bonded to the nitrogen in the Me_3NH^+ ion points toward the layers, suggesting the presence of hydrogen bonding to the selenides, see Fig. 2. The closest Se–H distances are Se(3)–H1 and Se(5)–H1 at 3.016 and 2.739 Å, respectively, which are much shorter than the van der Waals contact of 3.35 Å. Because the Me_3NH^+ cations are necessary for the formation of this phase they probably act as structure directing agents. Unfortunately, several

TABLE 9
Selected Angles (°) in the $[Ag_3As_2Se_5]_n^{n-}$ Layer with Standard Deviations in Parentheses

Se1–Ag1–Se2	108.6(1)	Ag1–Se3–Ag2	64.7(1)
Se1–Ag1–Se3	85.9(1)	Ag1–Se3–Ag2	110.6(1)
Se1–Ag1–Se5	116.7(1)	Ag2–Se3–Ag2	63.9(1)
Se2–Ag1–Se3	108.9(1)	Ag1–Se3–As1	119.0(1)
Se2–Ag1–Se5	119.8(1)	Ag2–Se3–As1	108.2(1)
Se3–Ag1–Se5	111.6(1)	Ag2–Se3–As1	94.4(1)
Se3–Ag2–Se3	116.1(1)	Ag2–Se4–As1	88.6(1)
Se3–Ag2–Se4	106.4(1)	Ag2–Se4–As2	86.5(1)
Se3–Ag2–Se5	115.2(1)	As1–Se4–As2	110.9(1)
Se3–Ag2–Se4	100.2(1)	Ag1–Se5–Ag2	68.4(1)
Se3–Ag2–Se5	113.0(1)	Ag1–Se5–Ag3	97.6(1)
Se4–Ag2–Se5	103.7(1)	Ag2–Se5–Ag3	125.6(1)
Se1–Ag3–Se2	124.7(1)	Ag1–Se5–As2	94.9(1)
Se1–Ag3–Se5	120.7(1)	Ag2–Se5–As2	110.4(1)
Se1–Ag3–As2	100.8(1)	Ag3–Se5–As2	123.3(1)
Se2–Ag3–Se5	93.2(1)	Se1–As1–Se3	100.1(1)
Se2–Ag3–As2	119.7(1)	Se1–As1–Se4	96.3(1)
Se5–Ag3–As2	95.0(1)	Se3–As1–Se4	102.9(2)
Ag1–Se1–Ag3	77.0(1)	Ag3–As2–Se2	116.2(1)
Ag1–Se1–As1	94.2(1)	Ag3–As2–Se4	139.6(1)
Ag3–Se1–As1	86.0(1)	Ag3–As2–Se5	99.5(1)
Ag1–Se2–Ag3	83.8(1)	Se2–As2–Se4	91.5(1)
Ag1–Se2–As2	91.2(1)	Se2–As2–Se5	98.5(1)
Ag3–Se2–As2	108.1(1)	Se4–As2–Se5	104.9(1)

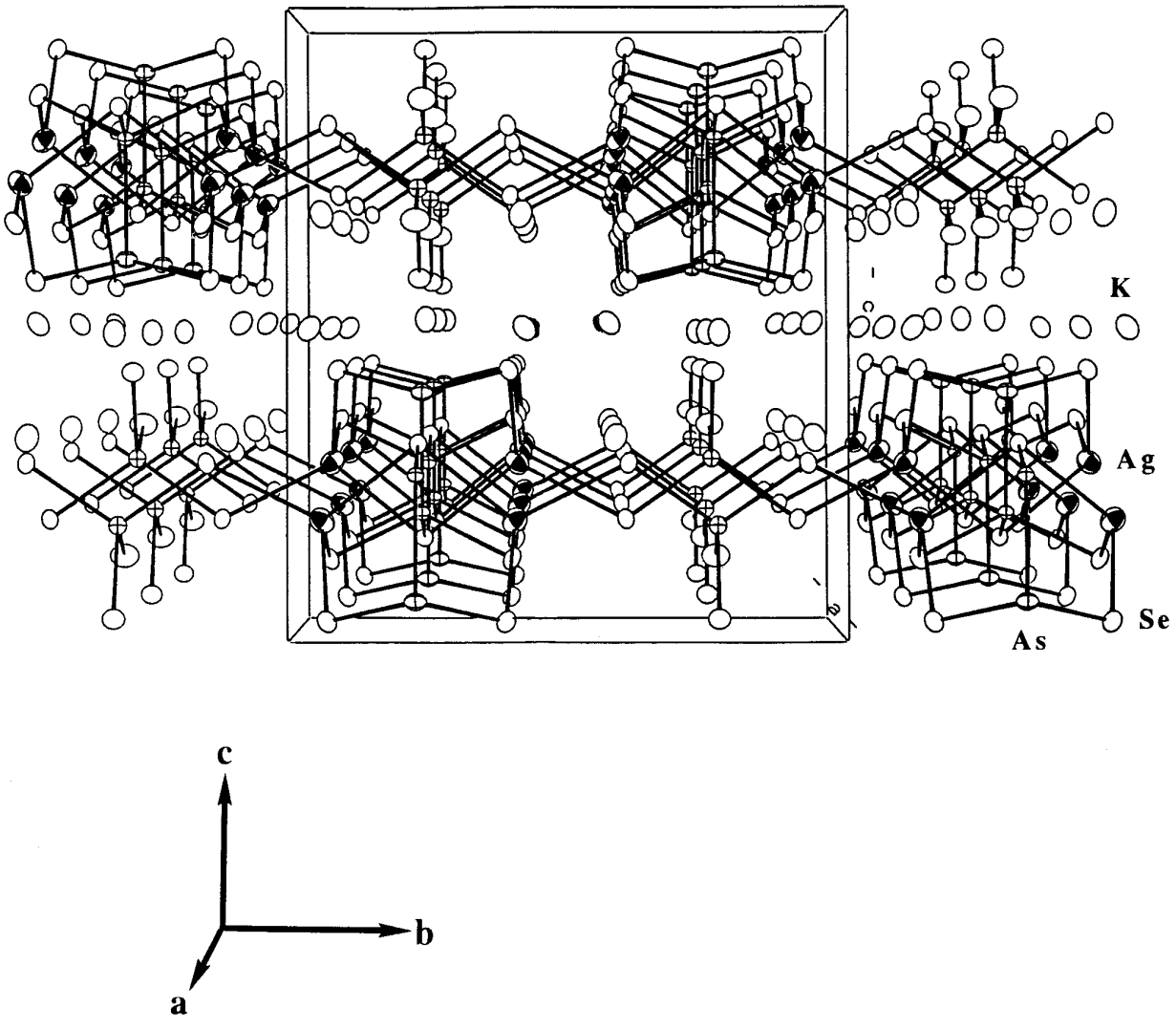

FIG. 4. Packing diagram of $K_5[Ag_2As_3Se_9]$ (III). Shaded circles are Ag, crossed circles are As, and open circles are Se and K.

attempts to perform ion-exchange reactions with this compound were unsuccessful.

Structure of $K_5[Ag_2As_3Se_9]$

This is a mixed-cation/mixed-$[As_xSe_y]^{n-}$ anion compound. The $[Ag_2As_3Se_9]_n^{5n-}$ macroanion has a unique two-dimensional layered structure with tetrahedral Ag^+ ions and two different types of selenoarsenate ligands, $[AsSe_4]^{3-}$ and $[As_2Se_5]^{4-}$; see Figs. 4 and 5. A more descriptive formula of the compound would be $[Ag_2(As_2Se_5)(AsSe_4)]$. The $[As_2Se_5]^{4-}$ unit here is different from the $[As_2Se_5]^{4-}$ unit found in $(Me_3NH)[Ag_3As_2Se_5]$. They are structural isomers. The $[As_2Se_5]^{4-}$ unit in $K_5[Ag_2As_3Se_9]$ can be viewed as the internal two-electron transfer (Scheme 4) product of the $[As_2Se_5]^{4-}$ unit found in $(Me_3NH)[Ag_3As_2Se_5]$. The formal oxidation state of the four-coordinated As atom can be assigned as 4+ while the three-coordinated As atom is 2+. The $[As_2Se_5]^{4-}$ (As–As bonded species (7b)) has been synthesized as a discrete anion in superheated ethylenediamine but again as far as we know this is the first example in a solid state material.

The structure of $[Ag_2As_3Se_9]_n^{5n-}$ can be described as chains of $[Ag_2As_2Se_5]^{2-}$ linked by tetrahedral $[AsSe_4]^{3-}$ units, see Fig. 6. A noteworthy feature of this compound is its mixed-valent As^{3+}/As^{5+} character. The Ag^+ ion is in a distorted tetrahedral environment with the Se–Ag–Se angles ranging from 103.65(9)° to 112.4(1)°. The average Ag-Se distance is normal at 2.693(3) Å. The average As–Se distance in the As^{3+} unit (i.e., $[As_2Se_5]^{4-}$), at 2.344(6) Å, is slightly longer than that of the As^{5+} unit (i.e., $[AsSe_4]^{3-}$), at 2.318(6) Å, as expected.

The $[AsSe_4]^{3-}$ uses only two of its four Se atoms to

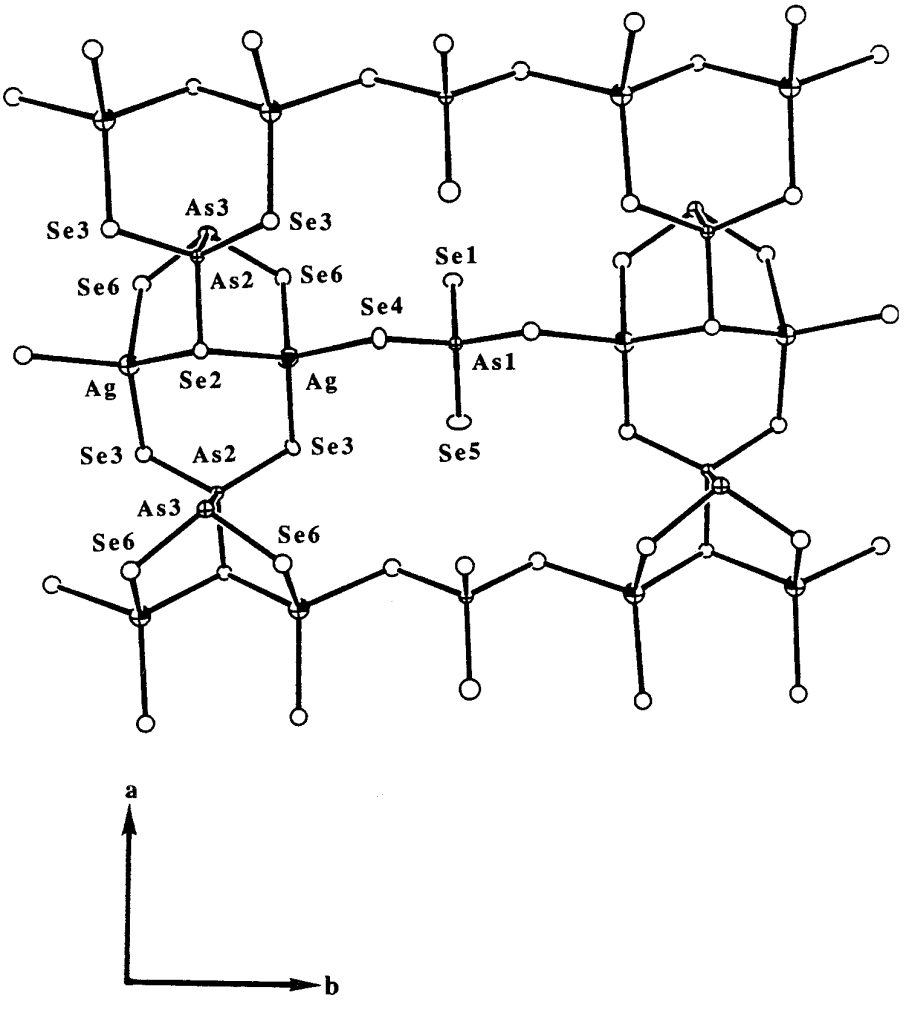

FIG. 5. Structure and labeling scheme of one $[Ag_2As_3Se_9]_n^{5n-}$ layer.

coordinate to Ag atoms and leaves the other two Se atoms as terminal selenides. The result of this bonding mode creates large 16-member rings where the K cations reside. The geometry of the seven-coordinated K(1) can best be described as trigonal prismatic with one of the faces capped by a seventh Se. The K(1)–Se distances range from 3.321(7) to 3.567(7) Å. The K(2) atom is also seven-coordinate with a capped trigonal antiprismatic environment. The K(2)–Se distances range from 3.247(6) to 3.588(6) Å. The six-coordinated K(3) has a distorted trigonal prismatic geometry with the K(3)–Se distances ranging from 3.346(9) to 3.423(8) Å. Selected bond distances and angles in the structure are summarized in Tables 10 and 11.

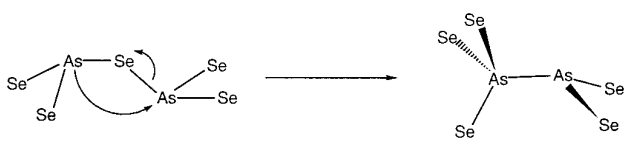

SCHEME 4. The isoelectronic relationship of the two discrete $[As_2Se_5]^{4-}$ anions.

Structure of $K[Ag_3As_2S_5]$

This compound is also a mixed cation/mixed anion salt. The structure contains unique two-dimensional layers of remarkable complexity, consisting of formally Ag^+ ions linked by a series of chain-like $[As_3S_7]^{5-}$ units and pyramidal $[AsS_3]^{3-}$ units, see Figs. 6 and 7. A more descriptive formula of the compound would be $K_2[Ag_6(AsS_3)(As_3S_7)]$. Although the $[As_3S_7]^{5-}$ units have been observed before in $[InAs_3S_7]^{2-}$, the binding mode is totally here. In $[InAs_3S_7]n^{2n-}$, the $[As_3S_7]^{5-}$ unit uses five of its terminal sulfur atoms to connect two In^{3+} centers, while in $[Ag_3As_2S_5]_n^{n-}$, the units are bonded to 10 Ag^+ centers, see Scheme 5.

There are three kinds of Ag atoms in the lattice. The

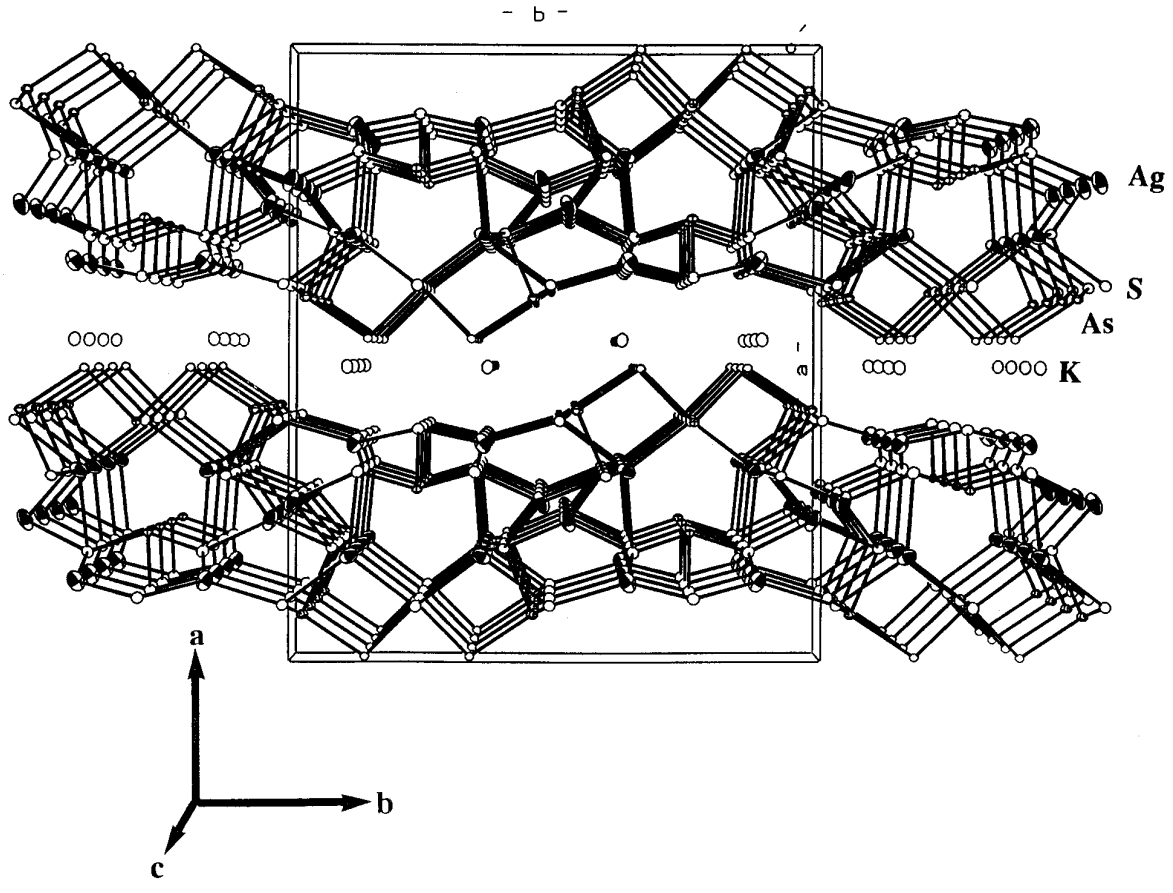

FIG. 6. Packing diagram of $K[Ag_3As_2S_5]$. Shaded circles are Ag, crossed circles are As, and open circles are S and K.

Ag(1) atom is in a distorted tetrahedral geometry with the S–Ag–S angles ranging from 101.5(2)° to 118.0(2)° while the Ag(2) and Ag(3) atoms are trigonal-planar coordinated to three S atoms. The Ag(2) atom is more distorted than the Ag(3) atom with S–Ag(2)–S angles ranging from 100.9(2)° to 155.1(1)°. The S–Ag(3)–S angles range from 110.8(2)° to 125.8(2)°. The angular distortions are probably due to the constrains imposed by the thioarsenate ligand. The average tetrahedral Ag(1)–S distance, at 2.638(6) Å, is longer than the average trigonal-planar Ag(2)–S and

TABLE 10
Selected Distances (Å) of $K_5[Ag_2As_3Se_9]$(III) with Standard Deviations in Parentheses

Ag–Se2	2.648(3)	K1–Se3	3.403(6)
Ag–Se3	2.683(3)	K1–Se4	3.567(7)
Ag–Se4	2.742(3)	K1–Se5	3.434(7)
Ag–Se6	2.699(3)	K1–Se6	3.489(6)
As1–Se1	2.313(6)	K2–Se1	3.294(6)
As1–Se4	2.340(3)	K2–Se3	3.385(6)
As1–Se5	2.302(5)	K2–Se4	3.476(5)
As2–Se2	2.356(3)	K2–Se4	3.380(5)
As2–Se3	2.346(3)	K2–Se5	3.337(6)
As3–Se6	2.331(3)	K2–Se6	3.247(6)
As1–As2	2.580(5)	K2–Se6	3.588(6)
K1–Se1	3.329(6)	K3–Se3	3.423(8)
K1–Se2	3.321(7)	K3–Se4	3.346(9)
K1–Se3	3.514(6)	K3–Se6	3.392(7)

TABLE 11
Selected Angles (°) in the $[Ag_2As_3Se_9]_n^{5n-}$ Layer with Standard Deviations in Parentheses

Se2–Ag–Se3	112.3(1)	Se1–As1–Se4	109.6(1)
Se2–Ag–Se4	110.6(1)	Se1–As1–Se5	107.8(2)
Se2–Ag–Se6	105.2(1)	Se4–As1–Se4	107.7(1)
Se3–Ag–Se4	112.4(1)	Se4–As1–Se5	111.1(1)
Se3–Ag–Se6	112.1(1)	Se2–As2–Se3	105.9(1)
Se4–Ag–Se6	103.65(9)	Se2–As2–Se3	110.2(2)
Ag–Se2–Ag	99.9(2)	Se3–As2–Se3	112.0(2)
Ag–Se2–As2	93.3(1)	Se3–As2–As3	111.3(1)
Ag–Se3–As2	105.1(1)	Se6–As3–Se6	105.8(2)
Ag–Se4–As1	114.5(1)	Se6–As3–As2	98.2(1)
Ag–Se6–As3	106.0(1)		

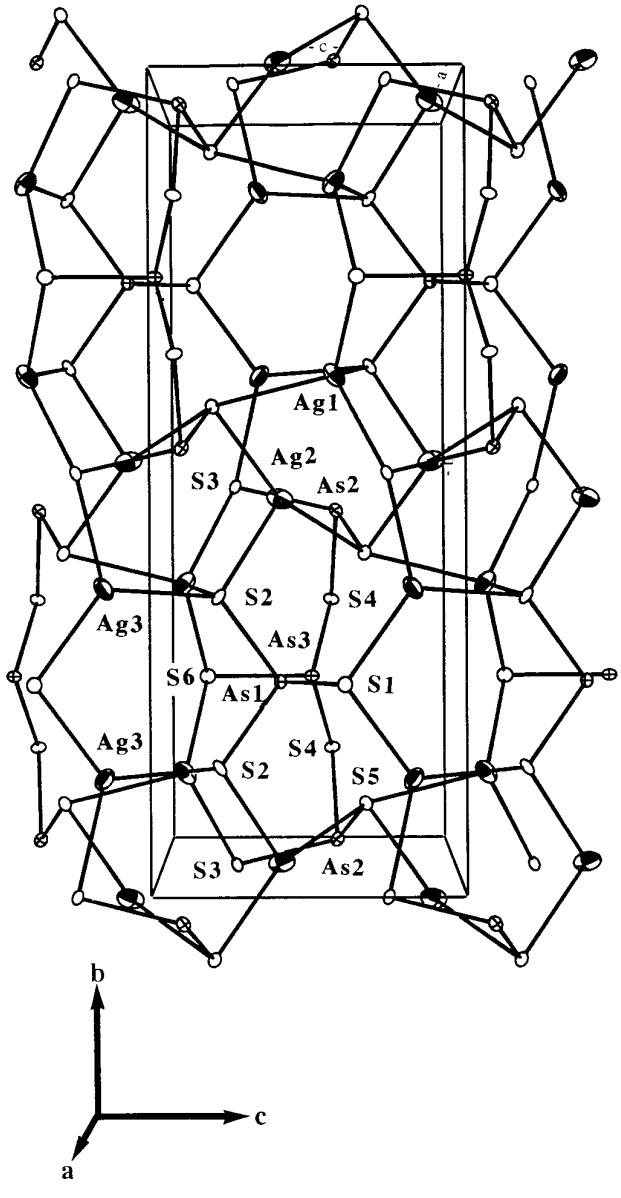

FIG. 7. Structure and labeling scheme of one $[Ag_3As_2S_5]_n^{n-}$ layer.

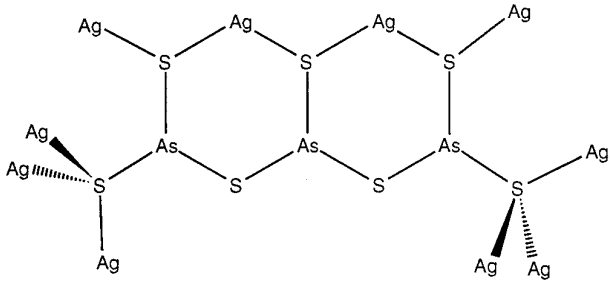

SCHEME 5

TABLE 12
Selected Distances (Å) of $K[Ag_3As_2Se_5]$ with Standard Deviations in Parentheses

Ag1–Ag2	2.996(3)	As1–S2	2.255(6)
Ag1–Ag2	3.139(3)	As2–S3	2.246(6)
Ag1–S2	2.620(6)	As2–S4	2.307(6)
Ag1–S3	2.758(6)	As2–S5	2.252(6)
Ag1–S5	2.624(6)	As3–S4	2.317(6)
Ag1–S6	2.550(6)	As3–S6	2.231(8)
Ag2–S2	2.568(7)	K–S1	3.150(8)
Ag2–S5	2.569(7)	K–S2	3.413(8)
Ag2–S5	2.538(7)	K–S3	3.299(8)
Ag3–S1	2.461(6)	K–S3	3.522(8)
Ag3–S2	2.488(6)	K–S4	3.269(8)
Ag3–S3	2.545(6)	K–S4	3.395(8)
As1–S1	2.238(9)	K–S6	3.302(9)

Ag(3)–S distances of 2.558(7) and 2.498(6) Å, respectively. The average As–S distances and S–As–S angles are normal at 2.268(6) Å and 99.5(2)° (9–12). The K atom is seven-coordinate with the K–S distances ranging from 3.150(8) to 3.522(8) Å. The coordination environment of K is irregular and can best be described as a capped trigonal antiprism. Selected distances and angles are summarized in Tables 12 and 13.

Thermal Properties

The thermal behavior of β-Ag_3AsSe_3 was investigated with differential thermal analysis (DTA); see Fig. 8. The DTA thermogram, first cycle, shows a melting point endotherm, at 396°C, and a crystallization point exotherm, at 342°C. The second cycle reveals two endothermic peaks, at 391 and 396°C, and the same crystallization point exotherm, at 342°C. Examination of the DTA residue by XRD

TABLE 13
Selected Angles (°) in the $[Ag_3As_2S_5]_n^{n-}$ Layer with Standard Deviations in Parentheses

S2–Ag1–S3	118.0(2)	S3–As2–S5	101.9(2)
S2–Ag1–S5	104.9(2)	S4–As2–S5	99.1(2)
S2–Ag1–S6	116.3(2)	S4–As3–S4	88.2(3)
S3–Ag1–S5	102.2(2)	S4–As3–S6	100.6(6)
S3–Ag1–S6	101.5(2)	S4–As3–S6	100.6(6)
S5–Ag1–S6	113.3(3)	Ag3–S1–As1	101.1(2)
S2–Ag2–S5	103.0(2)	Ag1–S2–As1	90.1(2)
S2–Ag2–S5	100.9(2)	Ag2–S2–As1	105.1(2)
S5–Ag2–S5	155.1(1)	Ag3–S2–As1	131.9(3)
S1–Ag3–S2	122.4(2)	Ag1–S3–As2	106.3(2)
S1–Ag3–S3	125.8(2)	Ag3–S3–As2	93.5(2)
S2–Ag3–S3	110.8(2)	As2–S4–As3	102.4(2)
S1–As1–S2	98.2(2)	Ag2–S5–As2	96.8(2)
S1–As1–S2	98.2(2)	Ag2–S5–As2	97.7(2)
S2–As1–S2	104.6(4)	Ag1–S6–As3	100.3(3)
S3–As2–S4	103.9(2)		

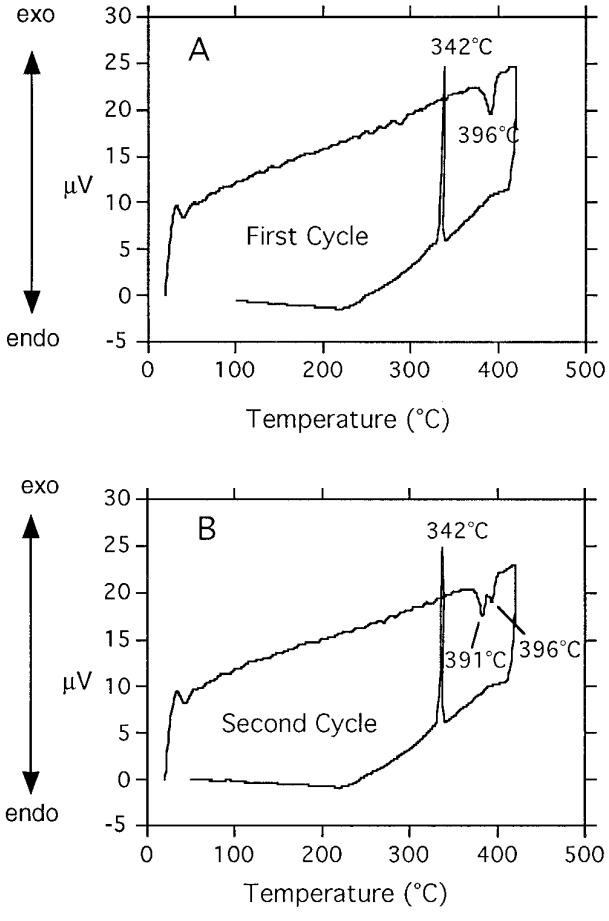

FIG. 8. DTA data for β-Ag_3AsSe_3. (A) First cycle. (B) Second cycle.

indicated that β-Ag_3AsSe_3 transformed into the α-Ag_3AsSe_3 with Ag_2Se as a minor product. The latter forms by the expulsion of As_2Se_3 from the material. This observation was also confirmed by the TGA experiment where β-Ag_3AsSe_3 loses mass around 250°C to give Ag_2Se; see Fig. 9. These data confirm that the β-form is kinetically stabilized.

The presence of Me_3NH^+ in the gallery space of II suggests that it may be possible to remove Me_3N by heating the material and obtain the solid acid product $HAg_3As_2Se_5$. Therefore, the thermal stability of $(Me_3NH)[Ag_3As_2Se_5]$ (II) was studied by TGA. There are two weight loss steps, one at 140–200°C and another at 430–770°C; see Fig. 10. The material, however, loses not only its organic cations as Me_3N but also H_2Se in a single step. The loss of structural selenium causes the destruction of the layers. The products were found to be, by X-ray powder diffraction, α-Ag_3AsSe_3 and $AgAsSe_2$. The second weight loss step corresponds to the evaporation of As_2Se_3. The final decomposition product was pure Ag_2Se(Ag_2Se-120, naumannite) (21). The size of the weight loss steps observed in the TGA diagram are in excellent agreement with the theoretical values.

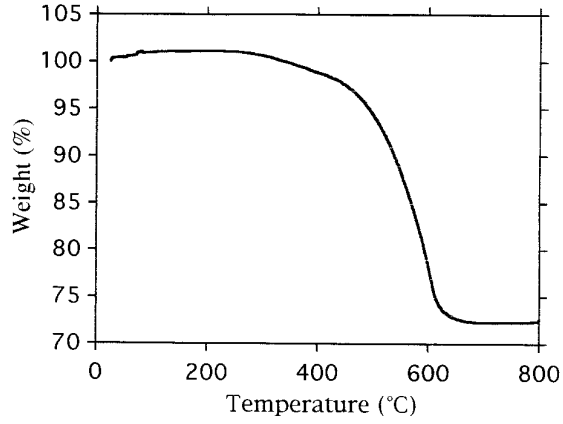

FIG. 9. TGA diagram of β-Ag_3AsSe_3.

The optical absorption spectra of the four compounds, in the range of 0.5 to 6 eV, show well-defined abrupt absorption edges from which the band gaps can be estimated; see Fig. 11. The optical gaps are 1.5, 2.5, 1.7, and 2.4 eV, for (I), (II), (III), and (IV), respectively, and indicate that these materials are semiconductors. It is noteworthy that the 1.5 eV value for β-Ag_3AsSe_3 is ideal for maximal efficiency for absorption of solar radiation and suggests that it may be a good candidate for examination as a photovoltaic material. Its semiconductor properties should be characterized if large high quality single crystals of this material could be grown.

CONCLUDING REMARKS

The synthesis of the new ternary and quaternary compounds, β-Ag_3AsSe_3, $(Me_3NH)[Ag_3As_2Se_5]$, $K_5[Ag_2As_3Se_9]$, and $K[Ag_3As_2S_5]$, attests that solvothermal technique is a powerful yet simple synthetic method in synthesizing new complex thio- and selenoarse-

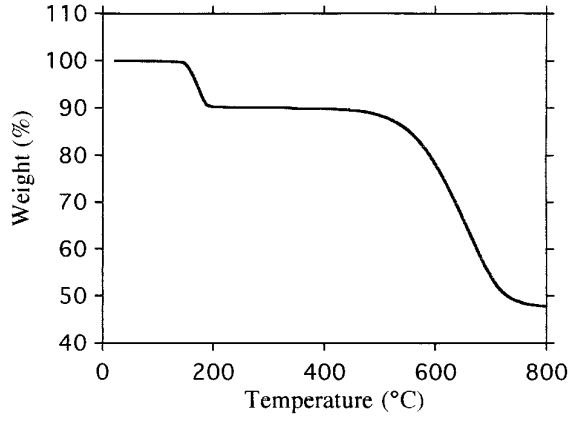

FIG. 10. TGA diagram of $(Me_3NH)[Ag_3As_2Se_5]$.

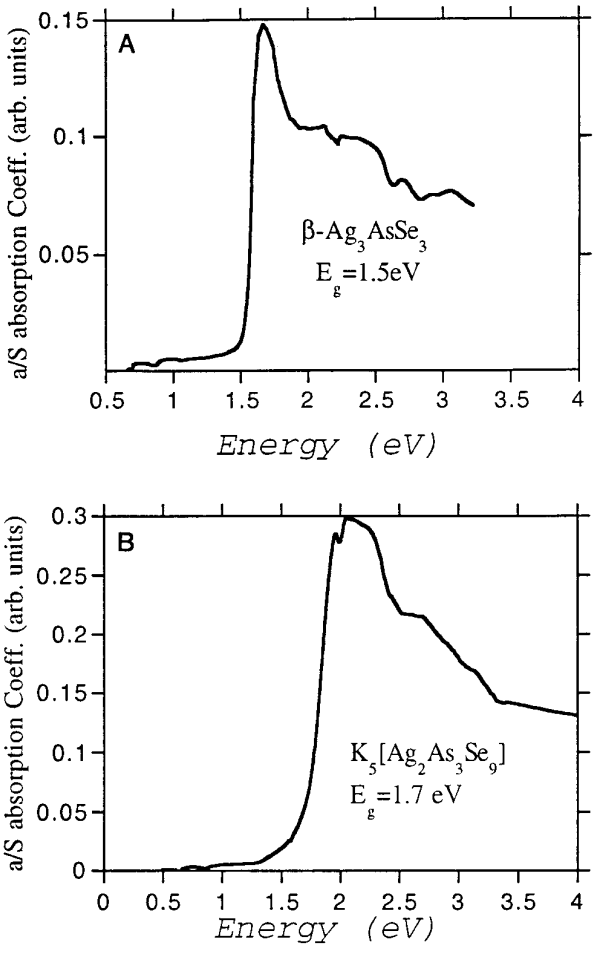

FIG. 11. Optical absorption spectra of (A) β-Ag_3AsSe_3 and (B) $K_5[Ag_2As_3Se_9]$.

nate compounds. As in other kinds of hydrothermal synthesis (i.e., zeolites, metal phosphates, etc.) the formation of these phases is closely linked not only to the preparation conditions but also the particular templating agents present. Perhaps more so in the compounds described here, the nature of the counterions dictates the kinetics of formation and the particular crystal lattice. There is no better demonstration of this than the case of $(Me_3NH)[Ag_3As_2Se_5]$, which forms even from a 99:1 mixture of Me_4N^+/ Me_3NH^+. The isolation of the metastable β-Ag_3AsSe_3, a new polymorph of a known mineral phase, implies that other low-temperature, kinetically stabilized, sulfosalt-like phases could be discovered in a similar fashion. The condensation of $[AsSe_3]^{3-}$ and $[AsS_3]^{3-}$ to higher order anions in protic solvents such as water and methanol proceeds readily as has been observed in previous systems (9–13). The formation of these anions is likely to be dictated by a number of factors, such as the pH, the nature of the metal, the nature of the counterion, and the solubility of the products. The most common mode of condensation involves corner sharing of the $[AsQ_3]^{3-}$ pyramids but other modes are also possible, such as the edge sharing of the pyramids in $(Ph_4P)_2[Ni_2As_4S_8]$ (12b). The degree of condensation also seems to vary between the sulfo- and the selenoanions, a reasonable behavior since they have different basicities. This chemical divergence sets the foundation for exploring both the S and Se species because isostructural phases between the two are not as likely.

ACKNOWLEDGMENT

We thank the Center for Fundamental Materials Research and from the National Science Foundation for financial support. We thank Dr. Arno Pfitzner for discussions.

REFERENCES

1. K. Volk and H. Schäfer, *Z. Anorg. Allg. Chem.* **414,** 220–230 (1975).
2. (a) B. Eisenmann and H. Schäfer, *Z. Naturforsch. B* **34,** 1637–1640 (1979); (b) H. Graf and H. Schäfer, *Z. Naturforsch. B* **34,** 383–385 (1979); (c) V. G. Dittmar and H. Schäfer, *Z. Anorg. Allg. Chem.* **441,** 93–97 (1978); (d) W. S. Sheldrick and H.-J. Haüsler, *Z. Anorg. Allg. Chem.* **557,** 105–111 (1988); (e) V. G. Dittmar and H. Schäfer, *Z. Anorg. Allg. Chem.* **441,** 98–102 (1978).
3. (a) W. S. Sheldrick and H.-J. Haüsler, *Z. Anorg. Allg. Chem.* **557,** 98–104 (1988); (b) W. S. Sheldrick and H.-J. Haüsler, *Z. Anorg. Allg. Chem.* **557,** 105–111 (1988); (c) W. S. Sheldrick and H.-J. Haüsler, *Z. Anorg. Allg. Chem.* **561,** 139–148 (1988); (d) W. S. Sheldrick and H.-J. Haüsler, *Z. Anorg. Allg. Chem.* **561,** 149–156 (1988); (e) W. Sheldrick and J. Kaub, *Z. Anorg. Allg. Chem.* **535,** 114–118 (1986); (f) W. Sheldrick and J. Kaub, *Z. Anorg. Allg. Chem.* **535,** 179–185 (1986).
4. (a) J. B. Parise, *Science*, **251,** 293–294 (1991); (b) J. B. Parise and Y. Ko, *Chem. Mater.* **4,** 1446–1450 (1992).
5. (a) P. T. Wood, W. T. Pennington, and J. W. Kolis, *Inorg. Chem.* **33,** 1556–1558 (1994); (b) J. E. Lerome, P. T. Wood, W. T. Pennington, and J. W. Kolis, *Inorg. Chem.* **33,** 1733–1734 (1994); (c) J. W. Kolis, personal communication.
6. (a) S. Dhingra and M. G. Kanatzidis, *Science*, **258,** 1769–1772 (1992); (b) J.-H. Liao and M. G. Kanatzidis, *J. Am. Chem. Soc.* **112,** 7400–7402 (1990); (c) J.-H. Liao and M. G. Kanatzidis, *Inorg. Chem.* **31,** 431–439 (1992); (d) K.-W. Kim and M. G. Kanatzidis, *J. Am. Chem. Soc.* **114,** 4878–4883 (1992); (e) K.-W. Kim and M. G. Kanatzidis, *J. Am. Chem. Soc.* **115,** 5871–5872 (1993).
7. (a) S.-P. Huang and M. G. Kanatzidis, *Coord. Chem. Rev.* **130,** 509–621 (1994); (b) L. C. Roof and J. W. Kolis, *Chem. Rev.* **93,** 1037–1080 (1993).
8. B. Siewert and U. Müller, *Z. Anorg. Allg. Chem.* **595,** 211–215 (1991).
9. J.-H. Chou and M. G. Kanatzidis, *Inorg. Chem.* **33,** 1001–1002 (1994).
10. J.-H. Chou and M. G. Kanatzidis, *Chem. Mater.* **7,** 5–8 (1995).
11. J.-H. Chou and M. G. Kanatzidis, *Inorg. Chem.* **33,** 5372–5373 (1994).
12. (a) J.-H. Chou and M. G. Kanatzidis, *J. Solid State Chem.* **123,** 115–122 (1996); (b) J.-H. Chou, J. A. Hanko, and M. G. Kanatzidis, *Inorg. Chem.,* in press.
13. (a) H.-O. Stephan and M. G. Kanatzidis, manuscript in preparation; (b) J.-H. Chou and M. G. Kanatzidis, submitted for publication.
14. K. Sakai, T. Koide, and T. Matsumoto, *Acta Crystallogr. B.* **34,** 3326–3328 (1978).
15. (a) G. M. Sheldrick, *in* "Crystallographic Computing 3" (G. M. Sheldrick, C. Kruger, and R. Goddard, Eds.), pp. 175–189. Oxford Univ. Press. Oxford, UK, 1985; pp 175–189; (b) "TEXSAN: Single Crystal

Structure Analysis Package,'' Version 5.0, Molecular Structure Corp., Woodland, TX.
16. N. Walker and D. Stuart, *Acta. Crystallogr. A* **39,** 158–166 (1983).
17. (a) D. M. Bogget and A. F. Gibson, *Phys. Lett.* **28,** 33–37 (1968); (b) M. Imafuku, I. Nakai, and K. Nagashima, *Mater. Res. Bull.* **21,** 493–501 (1986).
18. (a) A. Pfitzner, *Z. Anorg. Allg. Chem.* **620,** 1992–1997 (1994); (b) A. Pfitzner, *Z. Anorg. Allg. Chem.* **621,** 685–688 (1995).
19. G. W. Drake and J. W. Kolis, *Coord. Chem. Rev.* 131–178 (1994).
20. (a) W. Sheldrick and H.-J. Haüsler, *Z. Anorg. Allg. Chem.* **561,** 139–148 (1988); (b) W. Sheldrick and J. Kaub, *Z. Anorg. Allg. Chem.* **535,** 179–185 (1986); (c) S. C. O'Neal, W. T. Pennington, and J. W. Kolis, *J. Am. Chem. Soc.* **113,** 710–712 (1991); (d) S. C. O'Neal, W. T. Pennington, and J. W. Kolis, *Inorg. Chem.* **31,** 888–894 (1992).
21. JCPDS International Center for Diffraction Data, Powder Diffraction File 24–1044.